Desalination and Water Treatment
www.deswater.com

doi:10.5004/dwt.2017.20653

76 (2017) 98–111
May

Preparation and performance evaluation of cellulose acetate/nanodiamond nanocomposite membrane in the treatment of pharmaceutical wastewater by membrane bioreactor

Habib Etemadi[a,b], Reza Yegani[a,b,*], Mahdi Seyfollahi[a,b], Valiollah Babaeipour[c]

[a]*Faculty of Chemical Engineering,* [b]*Membrane Technology Research Center, Sahand University of Technology, Tabriz, Iran, email: etemadi.habib@yahoo.com (H. Etemadi), ryegani@sut.ac.ir (R. Yegani), m.seyfollahi.70@gmail.com (M. Seyfollah)*
[c]*Department of Biological Science and Technology, Malek Ashtar University of Technology, Tehran, Iran, email: vbabai@gmail.com (V. Babaeipour)*

Received 7 October 2016; Accepted 2 March 2017

ABSTRACT

Fabrication of less-fouling and high performance membrane is essential to offer significant cost reductions in membrane bioreactor (MBR) processes. In this regard, nanodiamond (ND) embedded cellulose acetate (CA) nanocomposite membrane was prepared and characterized in a lab-scale submerged MBR system for treating of pharmaceutical wastewater. In order to achieve efficient dispersion and providing more hydrophilic property, NDs were functionalized via heat treatment method. Scanning electron microscopy (SEM), and contact angle measurements were used to determine the surface properties of membranes. To compare the nanocomposite membranes with a pure CA membrane, critical flux, fouling behavior, and anti-fouling properties against extracellular polymeric substances (EPS) were investigated. SEM images showed that in the presence of 0.5 wt% of functionalized ND nanoparticles, porous structure appears on the membrane surfaces. The obtained results showed that in presence of functionalized NDs; ND-COOH, surface hydrophilicity of nanocomposite membrane was much higher than that of pristine CA membrane. Higher critical flux was obtained by CA/ND-COOH (0.5 wt.% of NDs) nanocomposite membrane due to the change of surface characteristics. The filamentous bacteria in the MBR resulted in more foulants on the CA membrane surface, while less filamentous bacteria were attached on the CA/ND-COOH nanocomposite membrane. Analysis of extractable EPS showed that the concentrations of proteins and carbohydrates in the EPS and soluble microbial products (SMP) for CA/ND-COOH (0.5 wt.%) membrane are less than other membranes. Also, COD removal for all of the membranes was higher than 90%, whereas only 83.4% removal efficiency was reached in the activated sludge.

Keywords: Cellulose acetate; Nanodiamond; Pharmaceutical wastewater; Membrane bioreactor; Antibiofouling

1. Introduction

Water scarcity has turned in to an issue for many areas in the world especially in hot and arid regions with limited water resources [1]. Water reuse is a pragmatic and sustainable approach to solve this problem and supply fresh water and also to help curb environmental pollution [2]. Pharmaceutical industry produce a variety of complex industrial wastes, which contain relatively high levels of suspended solids and soluble organics, many of which are recalcitrant [3,4]. Generally, the main part of these compounds cannot be completely removed by conventional activated sludge (CAS) treatment processes, due to the presence of solvents and organic compounds, which are often non-biodegradable or require longer time to be degraded [3,5–7].

In recent years, membrane bioreactor (MBR) has been playing a very important role in water and wastewater treatment [8]. MBR technology consists of intelligent com-

*Corresponding author.

bination of membrane and biological reactor systems [9], which has been widely utilized to treat both municipal and industrial wastewater due to its better effluent quality, high metabolic activity, small footprint demand and lower sludge production, when compared with CAS processes [10–15]. However, membrane fouling is still a major obstacle to widespread application of MBR, since it increases the hydraulic resistance to fluid flow and operating costs, resulting in less permeability and membrane life [11,16–18].

Membrane fouling is directly related to the adhesion of sludge matters such as bacteria and extracellular polymeric substances (EPS); large molecular weight compounds that are released by bacteria, on the membrane surface in MBR. Many reports indicate that the EPS is the most significant factor affecting fouling in MBR [19,20]. Hydrophilic modification of membrane materials and/or membrane surfaces can significantly decrease the membrane fouling [21]. Thus, it is highly desirable to have a membrane with antifouling capability, or anti-biofouling property. With respect to the hydrophobic property, membranes with hydrophilic nature, e.g. cellulose acetate (CA), potentially enhance the anti-fouling property.

CA is the foremost among polymer membranes. It has been widely used in separation processes and has been nominated as one of the most applicable polymers in preparation of membranes, due to its high hydrophilicity, high biocompatibility, non-toxic nature, good desalting, high potential flux and relatively low cost [22–24]. However, the high biofouling tendency and biodegradability are the main disadvantages of CA membranes in MBR medium, which necessitate the modification of CA [24,25].

Due to the rapid growth of nanotechnology, fabrication of nanocomposite membranes has shown to leave effects on their efficient performance over the past decades. In this regard, the effect of various nanoparticles on the engineering features of polymeric nanocomposite membranes has been extensively examined. In many cases a significant improvement in mechanical, thermal and antifouling properties has been seen. Thus, nanoparticle utilization can be regarded as an effective method in fouling reduction in MBR [21,26,27]. However, efficient and uniform dispersion of nanoparticles are largely governed by the interaction attractions that can be dominated to a great extent by the mixing process and the surface properties.

Carbon-based nanomaterials are potentially useful due to their unique physical and chemical properties. Among them, nanodiamond (ND) particles with a diamond core (sp^3 carbon-carbon bond) that is covered with multiple functional groups including carboxylic acids, hydroxyls, ketones, ethers, and lactones, are favored for many applications [28,29]. Because of the interesting characteristics of ND as well as its inherent hydrophilicity, [28,30,31], antibacterial activity [32,33], biocompatibility [34,35], chemical stability [34], thermal stability [35] non-toxicity [34–36], superior hardness, excellent mechanical properties, resistance to harsh environments [34] and ease of surface functionalization [35], it has been nominated as one of the most successful reinforcement fillers in the fabrication of nanocomposite materials. The non-diamond carbon from ND surface can be removed via thermal or acid treatments and some desirable functional groups, such as carboxyl groups can be easily formed, which could be beneficial to the dispersion capability of ND, especially in polar media [35,37].

ND nanoparticles have recently emerged as an important focus in the development of antibacterial and antibiofilm forming agents [38]. More recently, concern about the cytotoxic effects, aggregation and loss of antibacterial activity of some materials with antibacterial activity such as silver [39] has dramatically increased. In this case, our previous work has confirmed that ND can be used as a new effective agent against bacterial growth and prevent biodegradability of CA membrane [40]. Some oxygen-containing groups on the surface of ND, such as acid anhydrides, seem to be responsible for the antibacterial effect of the ND [33].

This research is focused on the fabrication of a nanocomposite membrane by incorporation of ND nanoparticle in the CA matrix and the evaluation of its performance in MBR. Also, as the dispersion of nanoparticles in the matrix strongly depend on efficient interaction between the polymer matrix and the nanoparticles, the pristine ND was functionalized via thermal treatment to create carboxyl groups on surface; which is denoted by ND-COOH. Nanocomposite membrane was fabricated by applying blending and phase inversion methods with different low concentrations of nanoparticles in order to enhance the membrane surface hydrophilicity and antifouling properties against EPS accumulation in MBR system under a short-term trial and sub-critical conditions. Prepared membranes were utilized in the bench scale developed MBR system to investigate waste treatment of a local pharmaceutical Co.

2. Experimental

2.1. Materials

Cellulose acetate (M_n = 30000), was supplied by Sigma-Aldrich (Germany) and was used as the basic polymer for the preparation of nanocomposite membrane. The detonation ND nanoparticle procured from Nabond technology Co., Ltd., China, having phase purity higher than 98% with an average diameter of 5 nm and a specific surface area of 282.8 m^2g^{-1} was used as nanoparticle. N-N-dimethylformamide (DMF, 99.8%) was purchased from Merck and used as a solvent to prepare dope solution. Deionized (DI) water was used as the non-solvents well as pure water for flux measurements.

2.2. Thermal oxidation of ND

First, as-received untreated ND were dried at 80°C for 2 h in vacuum dryer and then oxidized in air atmosphere at 430°C for 1.5 h according to literature [41], to remove organic impurities and enhance the surface carboxylic groups. Hereafter, the oxidized detonation ND is denoted by ND-COOH.

2.3. Preparation of nanocomposite membrane

The phase inversion technique was applied to prepare both neat and nanocomposite membranes. Dope solution containing 17.5 wt.% CA and 0.25–0.75 wt.% of ND or ND-COOH (the weight percentage of nanoparticles based on total polymer weight) in 82.5 wt.% DMF, was prepared.

First, ND and/or ND-COOH nanoparticles were dried at 80°C for 2 h under vacuum. This was performed to remove any possible physically absorbed moisture. After that, nanoparticles were added to DMF and stirred (Shimi Fan Company, Iran) for 4 h at room temperature. The mixture was sonicated (WOSON Company, China) at 50 kHz for 3 h to ensure a homogeneous spread of the nanoparticles and break up the agglomerates. Then CA (17.5 wt.%, by weight of the solution) was added to the initial mixture and dissolved in the solvent at 2000 rpm for 15 h. The dope solutions were then kept for 24 h to remove air bubbles followed by the casting on the glass plates by using automatic casting machine (Coa Test, Taiwan) at a constant shear rate and thickness of 10 mm/s and 200 μm, respectively. The cast films were subsequently immersed in a distilled water bath for 24 h to complete the phase separation process, where exchange between the solvent and non-solvent was carried out. The synthesized membranes were washed thoroughly with distilled water and kept in DI water to be ready for the following structural and operational characterization tests.

2.4. MBR set up and operational conditions

A lab-scale submerged MBR was used in this study. The rectangular tank of bioreactor was made by Plexiglas with the length, width and depth of 40, 30, and 30 cm, respectively. The total volume of the system was 36 L, and the effective volume was 12 L. Three flat sheet membrane modules were immersed in the activated sludge and were used in parallel under all operating conditions. An aeration pipe was installed underneath the membrane modules to provide oxygen for microorganisms and to create a shear force on the membrane surface to hinder the deposition of activated sludge particles. Fig. 1 shows three flat sheet modules submerged in the MBR test system.

The membrane-filtered effluent was extracted with a suction pump (OIL-LESS PISTON VACUUM, EP-40V model) connected to the membrane module. The influent wastewater and the adapted activated sludge were supplied from the wastewater treatment plant of Dana pharmaceutical company of Tabriz, Iran. The chemical oxygen demand (COD) of the utilized waste water stream was about 2800 mg/L.

The characteristics of the raw wastewater are shown in Table 1.

The three flat sheet membrane modules were made by polyamide with a volume capacity of 50 ml and an effective membrane surface area of 14.7 cm^2 [42]. Fig. 2 shows the flat-sheet membrane and frame configuration. The operation conditions are shown in Table 2. Mixed liquor suspended solids (MLSS) and volatile suspended solids (VSS) were measured as per the Standard Methods for Examination of Water and Wastewater (DIN 38 414).

2.5. Determination of critical flux

J_{crit} is the critical flux above which particles start to accumulate. It was determined by TMP-step method

Table 1
Characteristics of the pharmaceutical wastewater

Item	Value
Chemical oxygen demand (COD) (mg/L)	2800
Biochemical oxygen demand (BOD) (mg/L)	1490
BOD/COD	0.53
TKN (mg/L)	221
NH_3–N (mg/L)	108

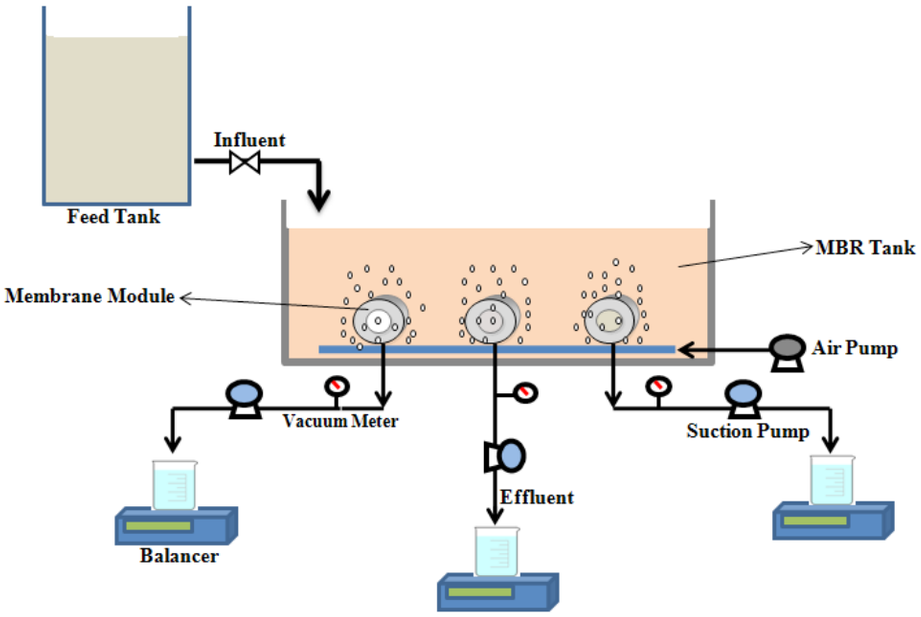

Fig. 1. Schematic diagram of the lab-scale MBR.

Fig. 2. Flat-sheet membrane and frame configuration.

Table 2
The operation conditions for the MBR test system

Parameters	Values
TMP (bar)	0.1 (sub-critical conditions)
HRT (h)	24
SRT (day)	25
Aeration ($m^3 m^{-2} h^{-1}$)	2.5–3
MLSS (mg/L)	6500–7000
Temperature (°C)	25

(variations of TMP via step by step technique) according to the method described by Gésan-Guiziou et al. [43]. In this method, TMP increases with time (30 min at each TMP step before J_{crit} was reached, 15 min afterwards), when J decreased over the course of time, leading to a non linearity in the $J = f$ (TMP) relationship, which means that the hydraulic resistance increased significantly due to deposition. The results could be separated into two flux groups, according to their different flux-TMP behaviors, i.e., lower flux group with little or no fouling and higher flux group with severe fouling. The intersection of two lines from each group was determined as the critical flux of the system. Thus, the critical values (TMP_{crit} and J_{crit}) can be determined, experimentally.

2.6. Extraction of EPS from membrane surface

The optimal EPS extraction method should be effective and not disrupt the EPS structure. The extraction efficiency for a given sample can be defined as the total amount of EPS extracted from the total organic matter. However, none of the extraction methods can completely extract the EPS from microbial aggregates [44]. In this work, the EPS solution was obtained by using the thermal treatment method. Thermal treatment method was known to be the most effective extraction method among the various proposed methods [45]. For this purpose, the membrane surface was first, rinsed with distilled water and the attached sludge on the membrane was taken out of the module, physically. In this case, two types of EPSs were separated, the loosely bound EPS (LB-EPS) and the tightly bound EPS (TB -EPS). The sample was centrifuged to remove the bulk solution (4000 rpm, 15 min), after which the supernatant, containing the soluble microbial products (SMP) fraction, was removed and then the sludge pellet was re-suspended with saline water (0.9% NaCl solution), followed by centrifugation under the same operating conditions [46,47]. The organic matter in the supernatant was regarded as the LB-EPS of the biomass. For the extraction of the TB-EPS, the sludge pellet left was suspended again, heated in a water bath (60°C, 30 min) and centrifuged at 4000 rpm for 15 min [47–49]. The collected supernatant was regarded as the TB-EPS. In order to measure the protein and carbohydrate contents, the extracted bound EPS and SMP were analyzed using Lowry's and Antrone's methods, respectively [50,51].

The bound EPS and SMP content were measured by analyzing the VSS of the solution. Fig. 3 shows a flowchart scheme of the methods described above.

2.7. Analysis of membrane fouling and fouling mechanism

After pure water flux (J_{w1}) tests, filtration of activated sludge for 6 h was carried out and then the membrane flux (J_{AS}) was measured. Thereafter, the fouled membranes were flushed with DI water and water flux was measured again (J_{w2}). In order to evaluate the membrane fouling, the flux recovery ratio (FRR) was calculated by using the following equation [24]:

$$FRR(\%) = \frac{J_{w2}}{J_{w1}} \times 100 \quad (1)$$

The flux loss caused by reversible (RFR), irreversible (IFR) and total fouling ratio (TFR) of the membrane in the filtration were defined by the following equations [52]:

$$RFR(\%) = \left(\frac{J_{w2} - J_{AS}}{J_{w1}} \right) \times 100 \quad (2)$$

$$IFR(\%) = \left(\frac{J_{w1} - J_{w2}}{J_{w1}} \right) \times 100 \quad (3)$$

$$TFR(\%) = RFR(\%) + IFR(\%) = \left(\frac{J_{w1} - J_{AS}}{J_{w1}} \right) \times 100 \quad (4)$$

The water quality was measured for the permeate water produced by the MBR process. COD was determined by absorbance method (Bio Quest CE2501).

2.8. Characterization of nanoparticle and membrnaes

2.8.1. Scanning electron microscopy (SEM)

The morphology of membrane samples was observed by scanning electron microscope (SEM, LEO model 1455VP, UK) operating at 15 Kv. In order to observe the membrane cross section, membrane samples were broken by using liquid nitrogen. For cross sectional images, membranes were fractured in liquid nitrogen. All the samples were gold-coated by sputtering to produce electrical conductivity.

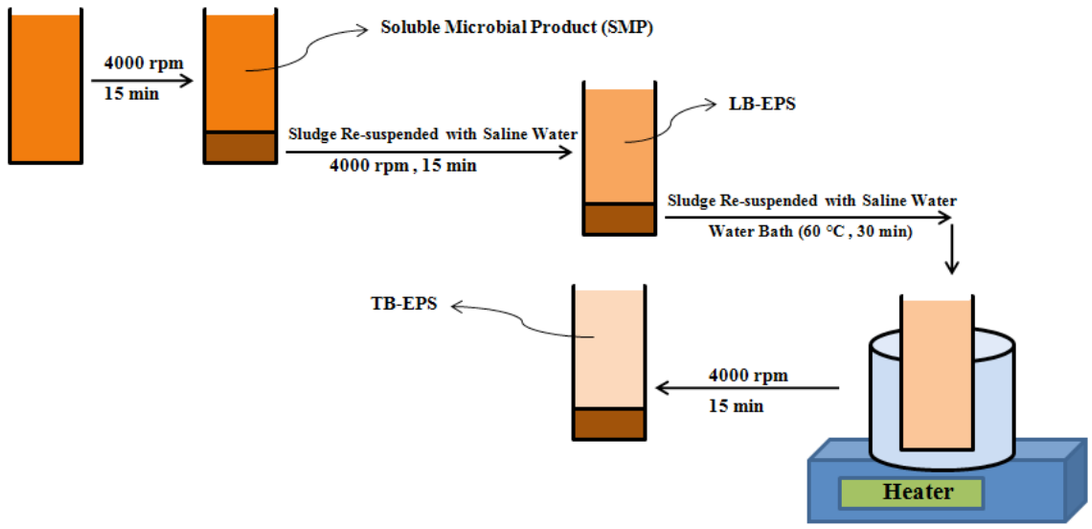

Fig. 3. Flow diagram of the applied protocol for the EPS heating extraction method.

2.8.2. Fourier transform infrared (FTIR) spectroscopy

The surface characterization of nanoparticles was performed by Fourier transform infrared spectroscopy (FTIR) analysis with a VERTEX 70 FTIR spectrometer (Bruker, Germany) in the range of 400–4000 cm^{-1}.

2.8.3. Contact angle measurement

The hydrophilicity of the membrane was determined by measuring the contact angle of the membrane surface with a contact angle goniometer (PGX, Thwing-Albert Instrument Co). At least five water contact angles at different locations on the membrane surface were recorded to get a reliable value

2.8.4. Water content

Water content (WC) tests were conducted to study the adsorption of water to the membranes containing the ND and ND-COOH nanoparticles. Pieces of different membrane samples were immersed in DI water at room temperature for 24 h and the weight of wetted membrane (W_{wet}) was measured after mopping with a filter paper. The dry weight (W_{dry}) was determined after 48 h drying at 75°C, the WC ratio was calculated by the following equation [53]:

$$WC\% = \frac{W_{wet} - W_{dry}}{W_{wet}} \times 100 \quad (5)$$

2.8.4. Membrane porosity

For porous membranes, the membrane porosity ε (%) could be determined by a gravimetric method, determining the weight of liquid contained in the membrane pores. The porosity of different membranes was calculated by Eq. (6) [54]:

$$\varepsilon(\%) = \frac{(W_w - W_d)/D_w}{(W_w - W_d)/D_w + W_d/D_p} \times 100 \quad (6)$$

where ε is the porosity of membrane (%), W_w is the wet sample weight (g), W_d is the dry sample weight (g), D_w (0.998 g cm^{-3}) and D_p (1.3 g cm^{-3})are the density of water and polymer at 25 °C, respectively.

3. Results and discussion

3.1. ND treatment characterization

FTIR analysis was carried out to characterize the surface chemistry of pristine ND and thermally treated ND; ND-COOH. Fig. 4 compares the FTIR spectra of ND and ND-COOH nanoparticles. Main characteristic peaks for ND are the absorption peaks at 2922.4 and 2860.7 cm^{-1} correspond to the asymmetric and symmetric stretching vibration of C–H band, respectively. Also, the absorption bands at 1341 cm^{-1} can be assigned to the deformation vibration of C–H band in alkyl group [55]. The absorption peak at 3423.8 cm^{-1} corresponds to the stretching vibration of O–H, while that at 1634.2 cm^{-1} corresponds to the deformation vibration of O–H band. The spectrum revealed another bands from oxygen containing functional groups, at 1711.4 and 1132.8 cm^{-1}, which are assigned to the stretching vibration of carbonyl, C=O and ether, C–O groups, respectively [56].

Comparing the FTIR spectra of pristine and thermally treated ND particles in Fig. 4 reveals that the variety of surface functional groups in pristine ND has been converted into their oxidized derivatives. After oxidation, for example, the C–H bands in ND completely disappeared and C=O vibrations bands are shifted from 1711.4 to 1796.2 cm^{-1}, indicating a conversion of ketones, aldehydes and esters groups into the carboxylic acids, anhydrides, or cyclic ketones groups. Upon the removal of graphitic layers by oxidation, the surface of ND becomes accessible for chemical reactions

and is immediately saturated with oxygen or oxygen-containing functional groups.

3.2. Membrane characterization

3.2.1. Membrane morphologies

SEM images were taken to determine the effects of ND and ND-COOH nanoparticles on the morphology of the CA membrane. Fig. 5 depicts the SEM micrographs of top surface of (a) CA, (b) CA/ND (0.5 wt.%) and (c) CA/ND-COOH (0.5 wt.%) membranes. These images confirm the non porous structure, as typical for CA membrane, which has been reported in many literatures [57–59]. It can be seen that in the presence of 0.5 wt% of both pure and functionalized ND nanoparticles, porous structure appears on the membrane surfaces.

SEM images of the cross-sections of the selected membranes; pure CA, CA/ND (0.5 wt.%) and CA/ND-COOH (0.5 wt.%) are shown in Fig. 6. All samples show asymmetric structure consisting of superior dense and inferior finger-like layers. It can be seen that in the presence of ND, the length of finger-like macropores increases and micro-cavities appear. The highly hydrophilic nature of CA strongly interacts with water as non-solvent and decreases its diffusion rate, which consequently retards the coagulation rate during the phase inversion process and results in the formation of denser skin layer [59]. With the addition of ND and ND-COOH particles, the number as well as the length of macrovoids increases, while the size of the macrovoids decreases after increasing ND and ND-COOH contents.

The pristine and functionalized NDs particles are not discernible in the cross sectional SEM images due to their relatively low content in the nanocomposite membranes. On the other hand, any ND and ND-COOH clusters or agglomerates are not observed in the SEM images of the membrane cross section (Figs. 6b and 6c) confirming the homogeneous dispersion of ND and ND-COOH particles in the CA membrane.

3.2.2. Hydrophilicity, porosity and water content of membranes

The surface hydrophilicity of membranes can affect the flux and antifouling ability of membranes. Table 3 shows the contact angle, porosity and water content (WC) of the neat and nancomposite membranes. To evaluate the surface hydrophilicity of the prepared membranes with different amounts of ND and ND-COOH particles, static surface contact angles of membranes were measured, and the obtained results are presented in Table 3. The CA membrane exhibited a low water contact angle of 65.4°, owing to its inherent hydrophilicity. The results show that the membranes hydrophilicity has been enhanced after adding ND and ND-COOH particles. When the ND particle content reaches to 0.5 wt.%, the water contact angle of nanocomposite membranes decreased to its minimum value; 58° and then increased with further addition of ND particles. In comparison with the CA/ND membrane, CA membrane with 0.5 wt.% of ND-COOH particles shows maximum decrease in water contact angle and reached 54°. Any further increase in ND-COOH content (>0.5 wt.%), increased the water contact angle. In other words, water contact angle of the membrane reduced to the lowest value due to the presence of –COOH functional groups of hydrophilic ND-COOH particles, which were well dispersed in the membrane. However, when the amount of ND or ND-COOH in aqueous phase is high enough, the distribution of nanoparticles becomes worse, leading to non-uniform dispersion, agglomeration and cluster formation of nanoparticles in the solution, which was reduces the effective surface of nanoparticles and functional groups on the surface of membranes [60]. This result proposes that the

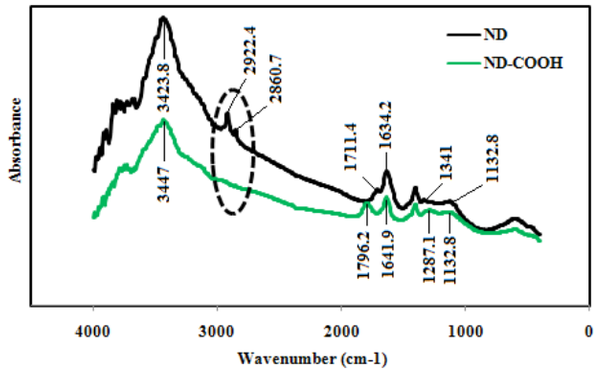

Fig. 4. FTIR spectra of ND and ND-COOH particles.

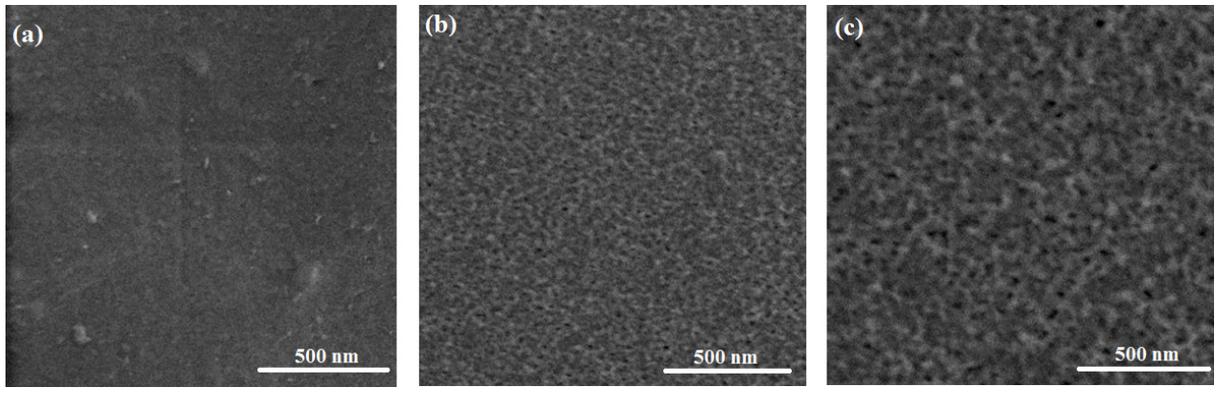

Fig. 5. SEM micrographs of top surface of: (a) CA, (b) CA/ND (0.5 wt.%) and (c) CA/ND-COOH (0.5 wt.%) membranes.

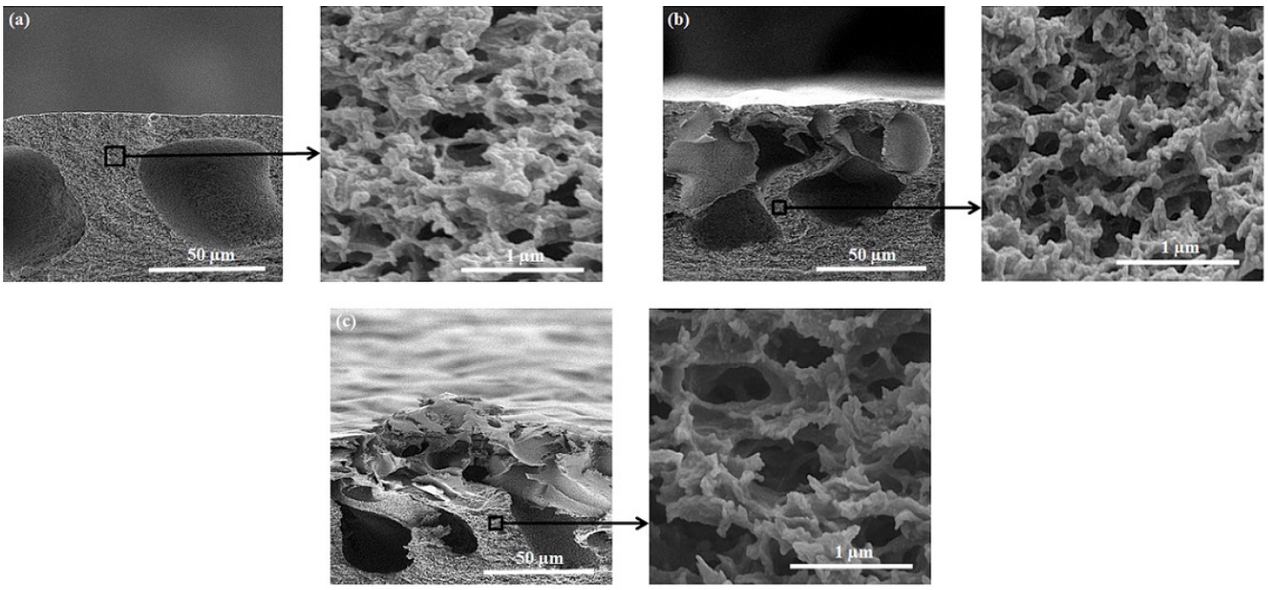

Fig. 6. The SEM images of the cross-sectional morphologies of the (a) CA, (b) CA/ND (0.5 wt.%) and (c) CA/ND-COOH (0.5 wt.%) membranes.

Table 3
Water contact angles, %WC and porosity for pure CA and its nanocomposite membranes

Membrane	Water contact angles (°)	Water content (%)	ε (%)
CA	65.4	71.6	76.7
CA/ND (0.25 wt.%)	60.3	74.2	78.6
CA/ND (0.5 wt.%)	58	75	80.5
CA/ND (0.75 wt.%)	59.1	73.5	78.5
CA/ND-COOH (0.25 wt.%)	57.7	75.5	80
CA/ND-COOH (0.5 wt.%)	54	76.1	81.4
CA/ND-COOH (0.75 wt.%)	59	75.2	80.1

hydrophilic ND and ND-COOH particles migrate spontaneously to the membrane surface and makes membrane surface hydrophilic [61]. Nanoparticles bundles have smaller specific surface area and lower adsorption activity with membrane surface. These findings are similar to other reports [52,60,62,63].

WC of the membrane is associated with the hydrophilicity of the membrane [57]. The WC was calculated according to the Eq. 5 and the obtained values were shown in Table 3. It is obvious that WC of pure CA membrane is 71.6% whereas for CA/ND membranes with 0.5 wt.% nanoparticles in the CA matrix WC increases to 75%, followed by a substantial decrease following any further increase in ND content. The increased WC may be due to the detachment of polymer chains from the ND surface, caused by interface voids. The membrane with 0.5 wt.% ND-COOH particles exhibited the maximum WC value; 76.1%. With any further increase in ND content, WC diminishes. A similar trend in WC has been reported by Liu et al. [64] when sulfonated mesoporous silica nanoparticles (SMSNs) were incorporated into sulfonated polyimides membrane.

The porosity of membranes has been measured by using gravimetric method and the results are depicted in Table 3. The existence of NPs results in a slight increase in the porosity of the nanocomposite membranes. It can be seen from Table 3 that by increasing the nanoparticles concentration, the porosity increases from 76.7% to 80.5% and 81.4% for CA, CA/ND (0.5 wt.%) and CA/ND-COOH (0.5 wt.%) membranes, respectively. Higher contents of ND as well as ND-COOH do not yield any further increase in the porosity of nanocomposite membranes. This finding can be attributed to particles agglomeration. However, mixing the hydrophilic nanoparticles with the CA matrix could enhance the volume fraction among the polymer chains, besides causing fast exchange of solvent and non-solvent during the phase inversion process.

3.2.3. Critical flux determination

The critical flux is the point, where the flux-TMP relationship becomes non-linear. The critical fluxes of membranes were measured by using the stepwise method. Fig. 7 shows the variation of permeation flux and transmembrane pressure (TMP), versus time for neat CA, CA/ND (0.5 wt.%) and CA/ND-COOH (0.5 wt.%) membranes. It can be seen from Fig. 7a that the mean permeate flux keeps a constant value of 19.2, 25.7, 34.2, and 42 L $m^{-2} h^{-1}$ during the operation of 30 min at the imposed TMP of 0.06, 0.08, 0.1, and 0.12 bar, respectively. When the imposed TMP reached up to 0.14 bar, the flux was exponentially decreased from 49.1 to 45.2 L $m^{-2} h^{-1}$. It is easy to understand that, the higher TMP conditions cause increment in the transport of particles and foulants toward the membrane surface and the accumulated layer becomes more compact, therefore, filtration flux is less than lower TMP or sub-critical conditions.

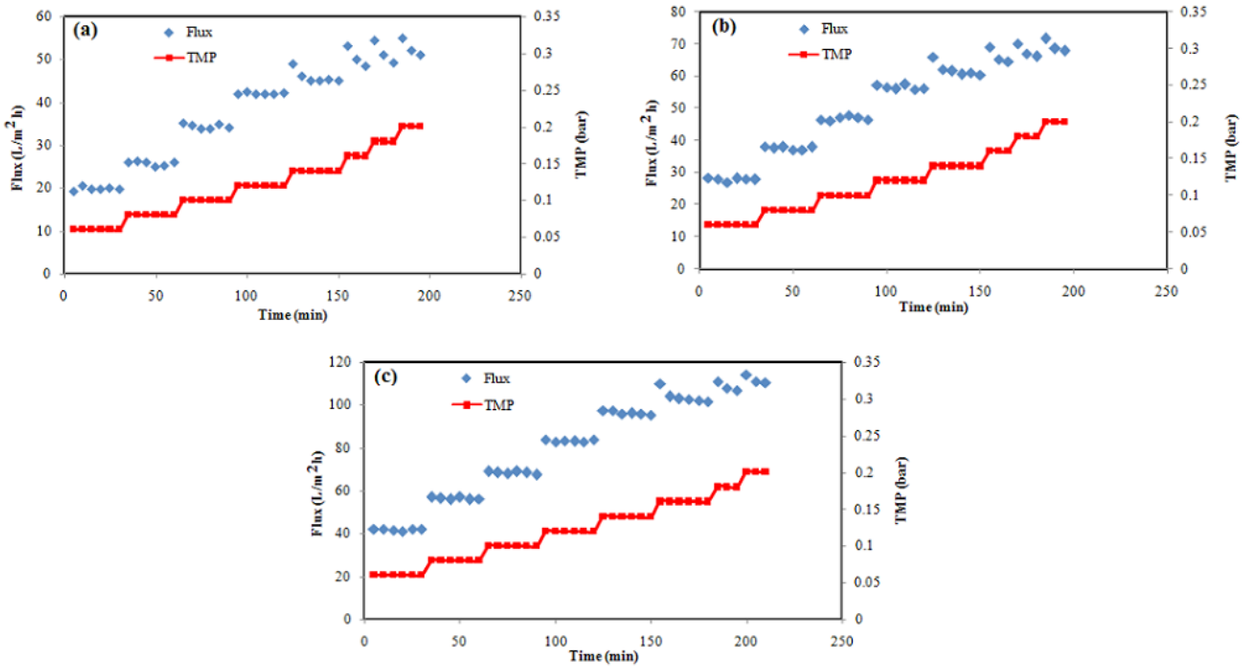

Fig. 7. Determination of the critical flux by the TMP-step method, permeation flux (J) and TMP versus time: (a) CA, (b) CA/ND (0.5 wt.%), and (c) CA/ND-COOH (0.5 wt.%).

This finding was similar to the results reported by Li et al. [65]. As shown in Fig. 7b and 7c, ND and ND-COOH nanoparticles have significant effects on the critical flux in submerged MBR. The hydrophilic and antibacterial ND nanoparticles (especially ND-COOH nanoparticles) improved the surface hydrophilicity and antibacterial activity of composite membranes, alleviating the interaction between foulants and membrane surface, and consequently enhancing membrane critical flux. It was reported that the membrane surface properties such as either hydrophilicity or hydrophobicity, have significant effects on the membrane permeability, membrane fouling and thus critical flux [26,49].

The variations of TMP vs. filtration flux during the measurement of critical point are shown in Fig. 8. For CA and CA/ND (0.5 wt.%) membranes, the first unstable point emerges in 0.14 bar, resulting in a non-linearity in the J = f (TMP) relationship. At this point, this phenomenon indicated the compressibility of the cake layer formed on the membrane surface [66], while the first unstable point for CA/ND-COOH (0.5 wt.%) membrane emerges in 0.16 bar. Thus, the critical fluxes of CA, CA/ND (0.5 wt.%) and CA/ND-COOH (0.5 wt.%) membranes in this experiment were determined as 44, 58.5 and 102 L $m^{-2} h^{-1}$, respectively.

However, regarding the super-critical flux, the transport of particles and foulants to the membrane surface will increase and the concentration polarization layer and/or cake layer will become more compact and thicker, resulting in more hydraulic resistance against the flow.

3.2.4. Fouling analysis and membrane performance

Flux decline behavior of the membranes during the filtration of mixed liquor in sub-critical conditions (TMP = 0.1 bar) is shown in Fig. 9. These results reveal that in comparison with neat CA membrane, flux has increased for both nanocomposite membranes. The permeation flux for CA/ND-COOH (0.5 wt.%) nanocomposite membrane is higher than other membrane. That indicates that the membrane hydrophilicity played the vital role in the improvement of the activated sludge flux. Any further decrease in permeate flux was caused by increasing the thickness of cake layer due to the deposition of additional foulant on the membrane surface. The slow trend of decline is due to operation in the sub-critical conditions, while for super critical condition, the sharp decline in flux is observed.

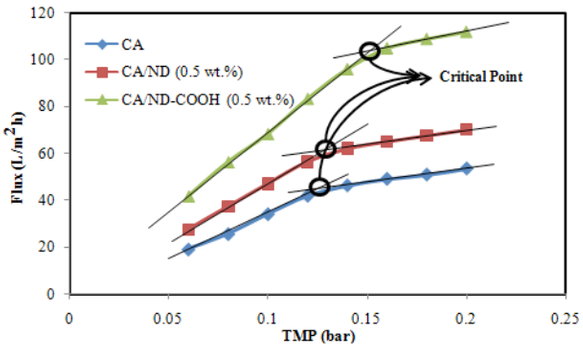

Fig. 8. Variations of TMP and filtration flux during the measurement of critical point.

Since all the membranes were tested at the same hydrodynamic condition, the difference in flux decline behavior is attributed to the only surface property of membrane.

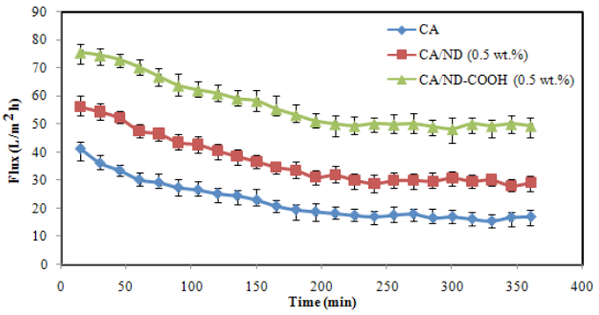

Fig. 9. Flux decline with operation time for CA, CA/ND (0.5 wt.%) and CA/ND-COOH (0.5 wt.%) membranes under sub-critical conditions and constant TMP (0.1 bar).

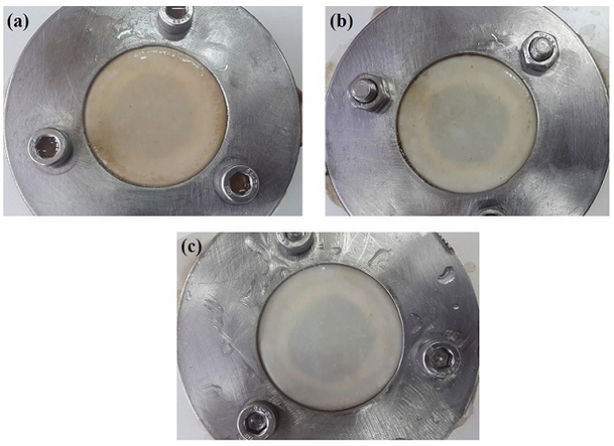

Fig. 10. Photographs of fouled membranes after MBR run in sub-critical conditions: (a) CA, (b) CA/ND (0.5 wt.%), and (c) CA/ND-COOH (0.5 wt.%) membranes.

According to Table 3, the surface of nanocomposite membranes are more hydrophilic than that of pure CA membrane, due to the presence of hydrophilic nanoparticles, i.e. ND and particularly ND-COOH. Therefore, hydrophobic adsorption between sludge particle and nanocomposite membranes was reduced.

Fig. 10 shows the photographs of fouled membranes surface after operation. This photograph indicates that the more foulants was attached on the fouled surface of CA membrane compared to CA/ND (0.5 wt.%) and CA/ND-COOH (0.5 wt.%) nanocomposite membranes. The hydrophilicity of the nanocompoite membrane surfaces also helps mitigate the adhesion of microorganism and microbial products due to their hydrophobic characteristics [67].

When a hydrophobic surface contacts a biological interface, biomolecules such as proteins show significant adsorption on the surface to minimize the interfacial energy, while a hydrophilic surface with low surface-water interfacial energy resists protein adsorption and cell adhesion [68]. Also, due to the antibacterial properties of ND and ND-COOH nanoparticles, nanocomposite membranes resist the adsorption of bacterial [40]. Therefore, the inhibition of biofouling was affected by the hydrophilicity and antibacterial properties of CA/ND (0.5 wt.%) and CA/ND-COOH (0.5 wt.%) nanocomposite membranes.

Microorganisms can be attached, grow on the membrane surface and produce enough extracellular polymeric substances (EPS) to facilitate the growth of a biofilm on the membrane surface. Fig. 11 shows the microscopic images of sludge flocs in mixed liquor and the attached filamentous bacteria on the membrane surfaces at the end of the test. It is revealed that the number of filamentous bacteria on the surface of CA/ND-COOH (0.5 wt.%) membrane is much less than other membranes. Choi et al. [17] reported that the filamentous bacteria produced more foulants than floc forming bacteria. The filamentous bacteria have a fixing action on the membrane foulants due to adhesion onto membrane surface [69]. The overgrowth of filamentous bacteria leads to a sharp increase in bound EPS concentration and then induces an increase in sludge viscosity and sludge hydrophobicity [70]. That is why the excess growth of filamentous bacteria resulted in the formation of a non-porous cake layer. Therefore, the filamentous bacteria played an important role in the membrane permeability.

Table 4
Fouling parameters of prepared membranes during activated sludge filtration under sub-critical conditions

Membrane	RFR (%)	IFR (%)	TFR (%)	FRR (%)
CA	77.5	15.5	93	84.5
CA/ND (0.5 wt.%)	76	12.9	88.9	87.1
CA/ND-COOH (0.5 wt.%)	76.3	7.8	84.1	92.2

Fouling analysis was made by calculating the reversible fouling ratio (RFR), irreversible fouling ratio (IFR), total fouling ratio (TFR), and flux recovery ratio (FRR) of membranes after activated sludge filtration test. These parameters are summarized in Table 4. All experimental data showed that RFR was the main fouling mechanism, and effect of IFR was negligible. Since all membranes were tested at the same condition, surface property of membrane was a key factor in determining the amount of TFR. Lower values of TFR exhibit that less foulant adsorption took place on the membrane surface or pore walls. When the membrane surface became more hydrophilic, the membrane's fouling was retarded, so the higher hydrophilicity and subsequently higher FRR of the CA/ND-COOH (0.5 wt.%) membranes created a lower fouling tendency than those of the CA and CA/ND (0.5 wt.%) membranes. According to Zhao et al. study [26], PVDF/GO composite membrane showed high antifouling properties in MBR media due to the hydrophilic properties of GO nanosheets, resulted in improved hydrophilicity of membrane surface. As shown in Table 4, the modification of CA membranes with ND-COOH nanoparticles improves its antifouling properties. This effect may be due to the negatively charged and hydrophilic skin layer of the nanocomposite membrane, which reduces the adsorption/plugging of foulants in the pore structure of nanocomposite membranes. Also, the antibacterial activity of nanocomposite membranes reduced the adsorption of bacteria on the membrane surface.

COD is the most important parameter which has been selected to assess the efficiency of a wastewater treatment process. COD removal of activated sludge and MBR was measured and illustrated in Fig. 12. The COD removal from supernatant was primarily due to biological degradation in the bioreactor while COD removal in the permeates was due to simulatouns impact of membrane filtration and biofilm formation (biofouling layer) on the membrane surfaces [3]. COD removals for all of the membranes were higher than 90%, whereas only 83.4% removal efficiency was obtained in the CAS bioreactor. That means the filtration membrane can effectively remove the COD and improve the effluent quality.

Results in Fig. 12 show that the pure CA membrane exhibited high COD removal compared to both nanocomposite membranes. As mentioned above, the membrane fouling was mostly attributed to the pore blocking as well as to the formation of a cake layer. Since the cake layer formed with the biofilm on the CA membrane surface was more dense than nanocomposite membranes, thus, it acts as a secondary membrane that filters and prevents the penetration of foulants (see Fig. 13) [71].

3.2.5. EPS analysis

It is well documented that the EPS is a controlling factor of membrane biofouling in MBR system [48,72]. The main fouling mechanisms of EPS include deposition, accumulation and consolidation of EPS on the membrane surfaces [73] and/or reduction in the permeability by filling the void spaces among cell particles [74]. SMP and soluble EPS are the same. SMP can be defined as the pool of organic compounds that are released into solution from substrate metabolism (usually with biomass growth) and biomass decay, while bound EPS has been reported as the major sludge floc components keeping the floc in a three-dimensional matrix [70,75,76]. The amounts of proteins and carbohydrates in terms of SMP, LB-EPS and TB-EPS accumulated on the membrane surfaces during the filtration test are shown in Fig. 14.

In Fig. 14a, the TB-EPS content in the cake layer on the surface of all membranes is the dominant foulant. By comparing the LB-EPS and TB-EPS in protein components for

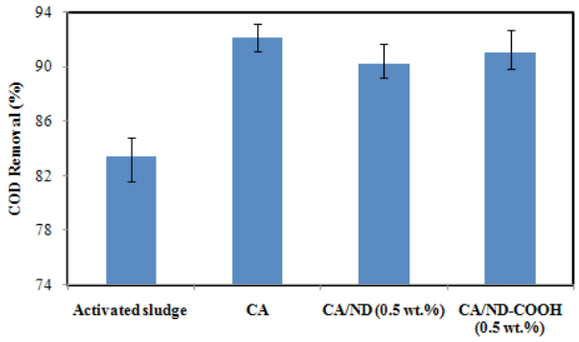

Fig. 12. COD removal percentage for activated sludge and membranes.

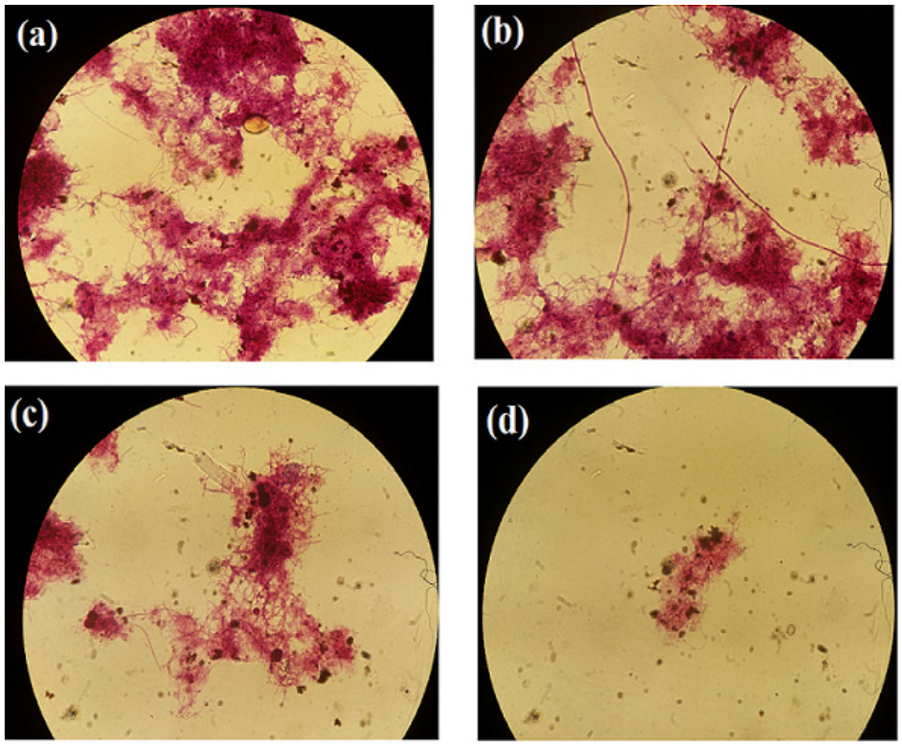

Fig. 11. Microscopic images of (a) sludge flocs in mixed liquor, (b) the attached filamentous bacteria on the CA, (c) CA/ND (0.5 wt.%) and (d) CA/ND-COOH (0.5 wt.%) membrane surfaces.

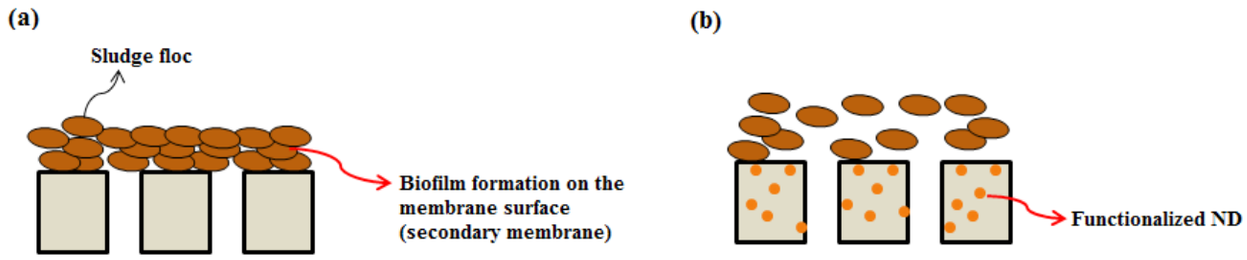

Fig. 13. Schematic illustration of biofilm formation on the membrane surface, (a) CA and (b) CA/ND-COOH membranes.

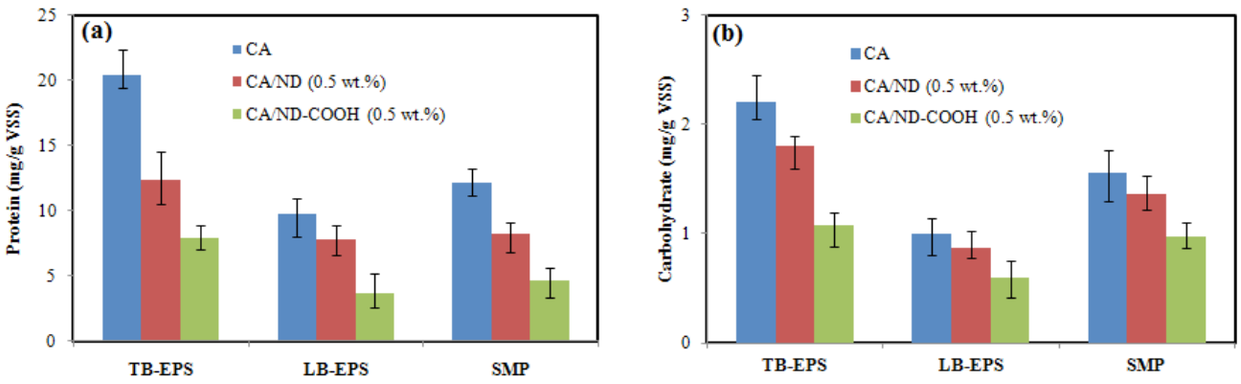

Fig. 14. SMP and bound EPS analysis of (a) proteins and (b) carbohydrates.

all of membranes, it could be easily found that the TB-EPS content was quite higher than that of LB-EPS content. The protein concentration in terms of bound EPS (LB-EPS and TB-EPS) on CA/ND-COOH (0.5 wt.%) nanocomposite membrane (11.6 mg/g VSS) was lower than that of CA/ND (0.5 wt.%) (20.24 mg/g VSS) and CA (30.18 mg/g VSS) membranes. The same behavior was observed for SMP on the membrane surfaces. SMP can be accumulated on the membrane surface or penetrate into the membrane pores. The concentration of proteins on the CA membrane surface was relatively higher than the both nanocomposite membranes in term of SMP for each membrane.

As shown in Fig. 14b, the trend of carbohydrate concentrations on the membrane surface is similar to the proteins. Carbohydrates are usually synthesized extracellular for a specific function, while proteins can exist in the extracellular polymer network due to the excretion of intracellular polymers or cell lysis [77]. The carbohydrate content of both LB-EPS and TB-EPS on CA membranes was 3.3 mg/g VSS, approximately 2 times higher than that of CA/ND-COOH (0.5 wt.%) nanocomposite membrane (1.68 mg/g VSS).

According to Jorand et al. [78], protein content mainly determines the hydrophobic characteristics while carbohydrate content usually determine the hydrophilic characteristics. Therefore, in this study, the SMP and EPS had hydrophobic properties. Hydrophobic interaction is generally considered as important mechanism regarding fouling [69]. This result proves that fouling in CA/ND-COOH (0.5 wt.%) membrane was reduced and less SMP and EPS, particularly carbohydrates, were adsorbed. Generally, carbohydrates can mediate cohesion of cells and play an important role in maintaining the structural integrity of biofilms. ND-COOH nanoparticles improved surface hydrophilicity of membrane. As a result, less amount of EPS, particularly polysaccharide was accumulated.

Sweity et al. [79] showed that the increased carbohydrates content on the membrane surface is proposed to be a result of stronger adherence properties of the EPS. As shown in Fig. 14b, CA/ND-COOH (0.5 wt.%) membrane has the lowest value in carbohydrates content with respect to other membranes. This means that CA/ND-COOH (0.5 wt.%) membrane shows weaker adherence with the EPS.

On the other hand, several studies have shown that SMP has a significant impact on the membrane fouling and scientific researches on SMP became one of the hot topics in membrane fouling [70,80–84]. However, in this study the SMP content of CA/ND-COOH (0.5 wt.%) nanocomposite membrane for both protein and carbohydrate is less than other membranes. In short, total EPS concentrations were generally one order of magnitude higher than those of SMP [3].

As shown in Fig. 14, the changing tendency of the carbohydrate and protein was similar to that of membrane fouling. This result indicates that EPS is one of the most influenced parameter of membrane fouling in MBR.

4. Conclusions

In this study, the antifouling behavior of pristine and heat treated nanodiamonds; ND and ND-COOH, embedded cellulose acetate (CA) nanocomposite membranes

during the filtration of pharmaceutical wastewater in bench-scale MBR system was investigated. The obtained results reveled that nanocomposite membrane fabricated by 0.5 wt.% ND-COOH embedded CA polymer exposes high hydrophilicity, high porosity and excellent antibiofouling properties and are suitable and promising membrane for MBR process. A video file supplied in the present work shows that the fouled membrane is easily cleaned either by tissue or rinsing by very slow water stream.

Analysis of extractable EPS showed that the concentrations of protein and carbohydrates in the EPS and SMP for CA/ND-COOH (0.5 wt.%) membrane is less than other membranes. The filamentous bacteria in the MBR resulted in a thick and dense cake layer on the CA membrane surface and these properties were the essential factors affecting membrane permeate flux. COD removals for all of the membranes were higher than 90%, whereas only 83.4% removal efficiency was obtained in the conventional activated sludge (CAS) system. As a final result, the CA/ND-COOH nanocomposite membrane showed excellent antifouling properties with respect to CA and CA/ND membranes, due to the presence of more hydrophilic groups (COOH) on the surface of ND-COOH particles.

Acknowledgement

The authors gratefully acknowledge financial support from Sahand University of Technology (grant no. 30/15975). The authors also gratefully acknowledge the technical supports and facilities, which were kindly supplied by Daana pharmaceutical company of Tabriz, Iran.

References

[1] J. Arevalo, L. Ruiz, J. Parada-Albarracin, D. González-Pérez, J. Pérez, B. Moreno, M. Gómez, Wastewater reuse after treatment by MBR. Microfiltration or ultrafiltration?, Desalination, 299 (2012) 22–27.

[2] S. Imran Khan, I. Hashmi, S.J. Khan, R. Henderson, Performance and optimization of lab-scale membrane bioreactors for synthetic municipal wastewater, Desal. Water Treat., 57 (2016) 1–8.

[3] Y. Kaya, G. Ersan, I. Vergili, Z.B. Gönder, G. Yilmaz, N. Dizge, C. Aydiner, The treatment of pharmaceutical wastewater using in a submerged membrane bioreactor under different sludge retention times, J. Membr. Sci., 442 (2013) 72–82.

[4] H.F. Schröder, Substance-specific detection and pursuit of non-eliminable compounds during biological treatment of waste water from the pharmaceutical industry, Waste Manage., 19 (1999) 111–123.

[5] I.A. Balcıoğlu, M. Ötker, Treatment of pharmaceutical wastewater containing antibiotics by O_3 and O_3/H_2O_2 processes, Chemosphere, 50 (2003) 85–95.

[6] S. Baumgarten, C. Charwath, M. Lange, S. Beier, J. Pinnekamp, Evaluation of advanced treatment technologies for the elimination of pharmaceutical compounds, Water Sci. Technol., 56 (2007) 1–8.

[7] R. López-Fernández, L. Martínez, S. Villaverde, Membrane bioreactor for the treatment of pharmaceutical wastewater containing corticosteroids, Desalination, 300 (2012) 19–23.

[8] M. Suresh Karthik Kumar, T. Krishna Kumar, P. Arulazhagan, S. Adish Kumar, I.-T. Yeom, J. Rajesh Banu, Effect of alkaline and ozone pretreatment on sludge reduction potential of a membrane bioreactor treating high-strength domestic wastewater, Desal. Water Treat., 55 (2015) 1127–1134.

[9] W. Luo, H.V. Pha, F.I. Hai, W.E. Price, W. Guo, H.H. Ngo, K. Yamamoto, L.D. Nghiem, Effects of salinity build-up on the performance and bacterial community structure of a membrane bioreactor, Bioresour. Technol., 200 (2015) 305–310.

[10] Z. Rahimi, A. Zinatizadeh, S. Zinadini, Preparation of high antibiofouling amino functionalized MWCNTs/PES nanocomposite ultrafiltration membrane for application in membrane bioreactor, J. Indust. Eng. Chem., 29 (2015) 366–374.

[11] L. Deng, W. Guo, H.H. Ngo, M.F.R. Zuthi, J. Zhang, S. Liang, J. Li, J. Wang, X. Zhang, Membrane fouling reduction and improvement of sludge characteristics by bioflocculant addition in submerged membrane bioreactor, Separ. Purif. Technol., 156 (2015) 450–458.

[12] F. Xie, W. Chen, J. Wang, J. Liu, Fouling characteristics and enhancement mechanisms in a submerged flat-sheet membrane bioreactor equipped with micro-channel turbulence promoters with micro-pores, J. Membr. Sci., 495 (2015) 361–371.

[13] C. Choi, M. Kim, E. Yang, I.S. Kim, Effects of aeration on/off times and hydraulic retention times in an intermittently aerated membrane bioreactor, Desal. Water Treat., 57 (2016) 7574–7581.

[14] I. Ali, S.-R. Kim, S.-P. Kim, J.-O. Kim, Recycling of textile wastewater with a membrane bioreactor and reverse osmosis plant for sustainable and cleaner production, Desal. Water Treat., 57 (2016) 1–9.

[15] K.-U. Do, R.J. Banu, D.-H. Son, I.-T. Yeom, Influence of ferrous sulfate on thermochemical sludge disintegration and on performances of wastewater treatment in a new process: Anoxic–oxic membrane bioreactor coupled with sludge disintegration step, Biochem. Eng. J., 66 (2012) 20–26.

[16] Y. Ding, Y. Tian, J. Liu, N. Li, J. Zhang, W. Zuo, Z. Li, Investigation of microbial structure and composition involved in membrane fouling in the forward osmosis membrane bioreactor treating anaerobic bioreactor effluent, Chem. Eng. J., 286 (2015) 198–207.

[17] J.-G. Choi, T.-H. Bae, J.-H. Kim, T.-M. Tak, A. Randall, The behavior of membrane fouling initiation on the crossflow membrane bioreactor system, J. Membr. Sci., 203 (2002) 103–113.

[18] J. Martín-Pascual, J. Leyva-Díaz, C. López-López, M. Muñio, E. Hontoria, J. Poyatos, Effects of temperature on the permeability and critical flux of the membrane in a moving bed membrane bioreactor, Desal. Water Treat., 53 (2015) 3439–3448.

[19] H. Lin, M. Zhang, F. Wang, F. Meng, B.-Q. Liao, H. Hong, J. Chen, W. Gao, A critical review of extracellular polymeric substances (EPSs) in membrane bioreactors: characteristics, roles in membrane fouling and control strategies, J. Membr. Sci., 460 (2014) 110–125.

[20] N. Thongmak, P. Sridang, U. Puetpaiboon, M. Héran, G. Lesage, A. Grasmick, Performances of a submerged anaerobic membrane bioreactor (AnMBR) for latex serum treatment, Desal. Water Treat., 57 (2015) 1–13.

[21] T.-H. Bae, T.-M. Tak, Effect of TiO_2 nanoparticles on fouling mitigation of ultrafiltration membranes for activated sludge filtration, J. Membr. Sci., 249 (2005) 1–8.

[22] N. Ghaemi, S.S. Madaeni, A. Alizadeh, P. Daraei, A.A. Zinatizadeh, F. Rahimpour, Separation of nitrophenols using cellulose acetate nanofiltration membrane: Influence of surfactant additives, Separ. Purif. Technol., 85 (2012) 147–156.

[23] N. Ghaemi, S.S. Madaeni, A. Alizadeh, P. Daraei, V. Vatanpour, M. Falsafi, Fabrication of cellulose acetate/sodium dodecyl sulfate nanofiltration membrane: Characterization and performance in rejection of pesticides, Desalination, 290 (2012) 99–106.

[24] J. Dasgupta, S. Chakraborty, J. Sikder, R. Kumar, D. Pal, S. Curcio, E. Drioli, The effects of thermally stable titanium silicon oxide nanoparticles on structure and performance of cellulose acetate ultrafiltration membranes, Separ. Purif. Technol., 133 (2014) 55–68.

[25] J.-H. Choi, S. Dockko, K. Fukushi, K. Yamamoto, A novel application of a submerged nanofiltration membrane bioreactor (NF MBR) for wastewater treatment, Desalination, 146 (2002) 413–420.

[26] C. Zhao, X. Xu, J. Chen, G. Wang, F. Yang, Highly effective antifouling performance of PVDF/graphene oxide composite membrane in membrane bioreactor (MBR) system, Desalination, 340 (2014) 59–66.
[27] M. Tavakolmoghadam, T. Mohammadi, M. Hemmati, F. Naeimpour, Surface modification of PVDF membranes by sputtered TiO_2: fouling reduction potential in membrane bioreactors, Desal. Water Treat., 57 (2016) 3328–3338.
[28] A. Krueger, The structure and reactivity of nanoscale diamond, J. Mater. Chem., 18 (2008) 1485–1492.
[29] Y.A. Haleem, D. Liu, W. Chen, C. Wang, C. Hong, Z. He, J. Liu, P. Song, S. Yu, L. Song, Surface functionalization and structure characterizations of nanodiamond and its epoxy based nanocomposites, Composites Part B: Eng., 78 (2015) 480–487.
[30] Y. Zhu, X. Xu, B. Wang, Z. Feng, Surface modification and dispersion of nanodiamond in clean oil, China Particuology, 2 (2004) 132–134.
[31] T. Huang, Y. Tzeng, Y. Liu, Y. Chen, K. Walker, R. Guntupalli, C. Liu, Immobilization of antibodies and bacterial binding on nanodiamond and carbon nanotubes for biosensor applications, Diam. Relat. Mater., 13 (2004) 1098–1102.
[32] O. Medina, J. Nocua, F. Mendoza, R. Gomez-Moreno, J. Avalos, C. Rodriguez, G. Morell, Bactericide and bacterial anti-adhesive properties of the nanocrystalline diamond surface, Diam. Relat. Mater., 22 (2012) 77–81.
[33] J. Wehling, R. Dringen, R.N. Zare, M. Maas, K. Rezwan, Bactericidal activity of partially oxidized nanodiamonds, ACS Nano, 8 (2014) 6475–6483.
[34] V.N. Mochalin, O. Shenderova, D. Ho, Y. Gogotsi, The properties and applications of nanodiamonds, Nature Nanotechnol., 7 (2012) 11–23.
[35] N.A. Burns, M.A. Naclerio, S.A. Khan, A. Shojaei, S.R. Raghavan, Nanodiamond gels in nonpolar media: Colloidal and rheological properties, J. Rheology (1978-present), 58 (2014) 1599–1614.
[36] K.B. Holt, Diamond at the nanoscale: applications of diamond nanoparticles from cellular biomarkers to quantum computing, Philos. Trans. Royal Soc. London A: Math. Phys. Eng. Sci., 365 (2007) 2845–2861.
[37] M.H. Avazkonandeh-Gharavol, S.A. Sajjadi, S.M. Zebarjad, M. Mohammadtaheri, M. Abbasi, M. Alimardani, K. Mossaddegh, Effect of heat treatment of nanodiamonds on the scratch behavior of polyacrylic/nanodiamond nanocomposite clear coats, Progr. Org. Coat., 76 (2013) 1258–1264.
[38] M. Khanal, V. Raks, R. Issa, V. Chernyshenko, A. Barras, J.M. Garcia Fernandez, L.I. Mikhalovska, V. Turcheniuk, V. Zaitsev, R. Boukherroub, Nanodiamonds: Selective antimicrobial and antibiofilm disrupting properties of functionalized diamond nanoparticles against Escherichia coli and Staphylococcus aureus (Part. Part. Syst. Charact. 8/2015), Part. Part. Syst. Charact., 32 (2015) 791–791.
[39] V. Turcheniuk, V. Raks, R. Issa, I.R. Cooper, P.J. Cragg, R. Jijie, N. Dumitrascu, L.I. Mikhalovska, A. Barras, V. Zaitsev, Antimicrobial activity of menthol modified nanodiamond particles, Diam. Relat. Mater., 57 (2015) 2–8.
[40] H. Etemadi, R. Yegani, V. Babaeipour, Study on the reinforcing effect of nanodiamond particles on the mechanical, thermal and antibacterial properties of cellulose acetate membranes, Diam. Relat. Mater., 69 (2016) 166–176.
[41] C.-C. Li, C.-L. Huang, Preparation of clear colloidal solutions of detonation nanodiamond in organic solvents, Colloids Surf. A: Physicochem. Eng. Asp., 353 (2010) 52–56.
[42] R. Yegani, H. Etemadi, M. Amini, Construction of membrane bioreactor system with high flexibility, Iranian pattent (in persian, pattent no. 85902), in: Iranian pattent (in persian, pattent no. 85902), Iran, 2015.
[43] G. Gesan-Guiziou, R. Wakeman, G. Daufin, Stability of latex crossflow filtration: cake properties and critical conditions of deposition, Chem. Eng. J., 85 (2002) 27–34.
[44] M.J. Brown, J.N. Lester, Comparison of bacterial extracellular polymer extraction methods, Appl. Environ. Microbiol., 40 (1980) 179–185.
[45] I.-S. Chang, C.-H. Lee, Membrane filtration characteristics in membrane-coupled activated sludge system—the effect of physiological states of activated sludge on membrane fouling, Desalination, 120 (1998) 221–233.
[46] J.R. Banu, D. Uan, S. Kaliappan, I. Yeom, Effect of sludge pretreatment on the performance of anaerobic/anoxic/oxic membrane bioreactor treating domestic wastewater, Int. J. Environ. Sci. Technol., 8 (2011) 281–290.
[47] L. Domínguez, M. Rodríguez, D. Prats, Effect of different extraction methods on bound EPS from MBR sludges. Part I: influence of extraction methods over three-dimensional EEM fluorescence spectroscopy fingerprint, Desalination, 261 (2010) 19–26.
[48] Z. Wang, Z. Wu, S. Tang, Extracellular polymeric substances (EPS) properties and their effects on membrane fouling in a submerged membrane bioreactor, Water Res., 43 (2009) 2504–2512.
[49] P. Le-Clech, V. Chen, T.A. Fane, Fouling in membrane bioreactors used in wastewater treatment, J. Membr. Sci., 284 (2006) 17–53.
[50] W. Trevelyan, R. Forrest, J. Harrison, Determination of yeast carbohydrates with the anthrone reagent, Nature, 170 (1952) 626–627.
[51] E.F. Hartree, Determination of protein: a modification of the Lowry method that gives a linear photometric response, Anal. Biochem., 48 (1972) 422–427.
[52] A. Khalid, A.A. Al-Juhani, O.C. Al-Hamouz, T. Laoui, Z. Khan, M.A. Atieh, Preparation and properties of nanocomposite polysulfone/multi-walled carbon nanotubes membranes for desalination, Desalination, 367 (2015) 134–144.
[53] M. Sivakumar, A. Mohanasundaram, D. Mohan, K. Balu, R. Rangarajan, Modification of cellulose acetate: Its characterization and application as an ultrafiltration membrane, J. Appl. Polym. Sci., 67 (1998) 1939–1946.
[54] M. Zhang, R.W. Field, K. Zhang, Biogenic silver nanocomposite polyethersulfone UF membranes with antifouling properties, J. Membr. Sci., 471 (2014) 274–284.
[55] Q. Zhang, K. Naito, Y. Tanaka, Y. Kagawa, Grafting polyimides from nanodiamonds, Macromolecules, 41 (2008) 536–538.
[56] J.-Y. Lee, D.-P. Lim, D.-S. Lim, Tribological behavior of PTFE nanocomposite films reinforced with carbon nanoparticles, Composites Part B: Eng., 38 (2007) 810–816.
[57] G. Arthanareeswaran, T.S. Devi, M. Raajenthiren, Effect of silica particles on cellulose acetate blend ultrafiltration membranes: Part I, Separ. Purif. Technol., 64 (2008) 38–47.
[58] T. Kusworo, J.S. Budiyono, D. Hakika, Enhanced Separation performance of cellulose acetate membrane for brackish water separation using modification of additives and thermal annealing, Int. J. Waste Resour., 4 (2014) 1–9.
[59] W. Chen, Y. Su, L. Zhang, Q. Shi, J. Peng, Z. Jiang, In situ generated silica nanoparticles as pore-forming agent for enhanced permeability of cellulose acetate membranes, J. Membr. Sci., 348 (2010) 75–83.
[60] Z. Xu, J. Zhang, M. Shan, Y. Li, B. Li, J. Niu, B. Zhou, X. Qian, Organosilane-functionalized graphene oxide for enhanced antifouling and mechanical properties of polyvinylidene fluoride ultrafiltration membranes, J. Membr. Sci., 458 (2014) 1–13.
[61] J.-H. Choi, J. Jegal, W.-N. Kim, Fabrication and characterization of multi-walled carbon nanotubes/polymer blend membranes, J. Membr. Sci., 284 (2006) 406–415.
[62] E. Yuliwati, A.F. Ismail, T. Matsuura, M.A. Kassim, M.S. Abdullah, Effect of modified PVDF hollow fiber submerged ultrafiltration membrane for refinery wastewater treatment, Desalination, 283 (2011) 214–220.
[63] G. Zhang, S. Lu, L. Zhang, Q. Meng, C. Shen, J. Zhang, Novel polysulfone hybrid ultrafiltration membrane prepared with TiO 2-g-HEMA and its antifouling characteristics, J. Membr. Sci., 436 (2013) 163–173.
[64] D. Liu, L. Geng, Y. Fu, X. Dai, C. Lü, Novel nanocomposite membranes based on sulfonated mesoporous silica nanoparticles modified sulfonated polyimides for direct methanol fuel cells, J. Membr. Sci., 366 (2011) 251–257.

[65] X. Li, J. Li, J. Wang, H. Wang, B. He, H. Zhang, Ultrasonic visualization of sub-critical flux fouling in the double-end submerged hollow fiber membrane module, J. Membr. Sci., 444 (2013) 394–401.
[66] S. Chellam, W. Xu, Blocking laws analysis of dead-end constant flux microfiltration of compressible cakes, J. Colloid Interf. Sci., 301 (2006) 248–257.
[67] J. Lee, H.-R. Chae, Y.J. Won, K. Lee, C.-H. Lee, H.H. Lee, I.-C. Kim, J.-m. Lee, Graphene oxide nanoplatelets composite membrane with hydrophilic and antifouling properties for wastewater treatment, J. Membr. Sci., 448 (2013) 223–230.
[68] S. Krishnan, C.J. Weinman, C.K. Ober, Advances in polymers for anti-biofouling surfaces, J. Mater. Chem., 18 (2008) 3405–3413.
[69] F. Meng, H. Zhang, F. Yang, Y. Li, J. Xiao, X. Zhang, Effect of filamentous bacteria on membrane fouling in submerged membrane bioreactor, J. Membr. Sci., 272 (2006) 161–168.
[70] F. Meng, S.-R. Chae, A. Drews, M. Kraume, H.-S. Shin, F. Yang, Recent advances in membrane bioreactors (MBRs): membrane fouling and membrane material, Water Res., 43 (2009) 1489–1512.
[71] C. Wang, W.-N. Chen, Q.-Y. Hu, M. Ji, X. Gao, Dynamic fouling behavior and cake layer structure changes in nonwoven membrane bioreactor for bath wastewater treatment, Chem. Eng. J., 264 (2015) 462–469.
[72] S. Annop, P. Sridang, U. Puetpaiboon, A. Grasmick, Influence of relaxation frequency on membrane fouling control in submerged anaerobic membrane bioreactor (SAnMBR), Desal. Water Treat., 52 (2014) 4102–4110.
[73] H. Nagaoka, S. Ueda, A. Miya, Influence of bacterial extracellular polymers on the membrane separation activated sludge process, Water Sci. Technol., 34 (1996) 165–172.
[74] P. Hodgson, G. Leslie, A. Fane, R. Schneider, C. Fell, K. Marshall, Cake resistance and solute rejection in bacterial microfiltration: the role of the extracellular matrix, J. Membr. Sci., 79 (1993) 35–53.
[75] A. Yuniarto, Z.Z. Noor, Z. Ujang, G. Olsson, A. Aris, T. Hadibarata, Bio-fouling reducers for improving the performance of an aerobic submerged membrane bioreactor treating palm oil mill effluent, Desalination, 316 (2013) 146–153.
[76] S. Feng, N. Zhang, H. Liu, X. Du, Y. Liu, H. Lin, The effect of COD/N ratio on process performance and membrane fouling in a submerged bioreactor, Desalination, 285 (2012) 232–238.
[77] L. Duan, W. Jiang, Y. Song, S. Xia, S.W. Hermanowicz, The characteristics of extracellular polymeric substances and soluble microbial products in moving bed biofilm reactor-membrane bioreactor, Bioresour. Technol., 148 (2013) 436–442.
[78] F. Jorand, F. Boue-Bigne, J. Block, V. Urbain, Hydrophobic/hydrophilic properties of activated sludge exopolymeric substances, Water Sci. Technol., 37 (1998) 307–315.
[79] A. Sweity, W. Ying, M.S. Ali-Shtayeh, F. Yang, A. Bick, G. Oron, M. Herzberg, Relation between EPS adherence, viscoelastic properties, and MBR operation: Biofouling study with QCM-D, Water Res., 45 (2011) 6430–6440.
[80] S. Rosenberger, C. Laabs, B. Lesjean, R. Gnirss, G. Amy, M. Jekel, J.-C. Schrotter, Impact of colloidal and soluble organic material on membrane performance in membrane bioreactors for municipal wastewater treatment, Water Res., 40 (2006) 710–720.
[81] E. Iritani, N. Katagiri, T. Sengoku, K. Yoo, K. Kawasaki, A. Matsuda, Flux decline behaviors in dead-end microfiltration of activated sludge and its supernatant, J. Membr. Sci., 300 (2007) 36–44.
[82] S. Liang, C. Liu, L. Song, Soluble microbial products in membrane bioreactor operation: behaviors, characteristics, and fouling potential, Water Res., 41 (2007) 95–101.
[83] R.C. Eusebio, Y.-H. Cho, M. Sibag, H.-G. Kim, T.-H. Chung, H.-S. Kim, Significant role of membrane fouling and microbial community on the performance of membrane bioreactor (MBR) system, Desal. Water Treat., 17 (2010) 90–98.
[84] Z. Pan, C. Zhang, B. Huang, Using adsorbent made from sewage sludge to enhance wastewater treatment and control fouling in a membrane bioreactor, Desal. Water Treat., 57 (2016) 9070–9081.